INTERNATIONAL JOURNAL OF HYDROGEN ENERGY XXX (2017) 1–12

Available online at www.sciencedirect.com

ScienceDirect

journal homepage: www.elsevier.com/locate/he

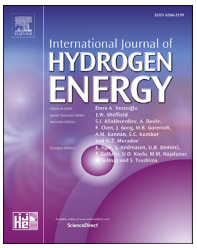

Perturbation estimation based robust state feedback control for grid connected DFIG wind energy conversion system

Bo Yang [a], *Yilin Hu* [a], *Haiyan Huang* [a], *Hongchun Shu* [a], *Tao Yu* [b,*], *Lin Jiang* [c]

[a] *Faculty of Electric Power Engineering, Kunming University of Science and Technology, 650500, Kunming, China*
[b] *School of Electric Power Engineering, South China University of Technology, Guangzhou, China*
[c] *Department of Electrical Engineering & Electronics, University of Liverpool, Liverpool, L69 3GJ, United Kingdom*

ARTICLE INFO

Article history:
Received 24 April 2017
Received in revised form
20 June 2017
Accepted 29 June 2017
Available online xxx

Keywords:
DFIG
MPPT
Perturbation estimation
State feedback control

ABSTRACT

This paper develops a perturbation estimation based robust state feedback control (PER-SFC) scheme of doubly-fed induction generator (DFIG) for maximum power point tracking (MPPT). The combinatorial effect of nonlinearities originally stemmed from wind turbine aerodynamics, generator modelling uncertainties and wind speed randomness is aggregated as a perturbation, which is rapidly estimated online by a sliding-mode state and perturbation observer (SMSPO). Then, a linear state feedback controller is designed to fully compensate the perturbation estimate in real-time. Furthermore, only the measurement of rotor speed and reactive power is needed while no accurate DFIG model is required by the proposed approach. Under such framework, the elegant merits of conventional linear state feedback control (favourable implementation simplicity and high reliability) and nonlinear robust control (global control consistency and considerable robustness) can be wisely incorporated. Meanwhile, their inherent drawbacks could be significantly reduced. Case studies are undertaken which verify the effectiveness and superiority of PER-SFC compared to that of other classical methods.

Introduction

In the past decade, fast global population booming and continuous environment deterioration have driven considerable social and industrial demands of renewable energy, hydrogen based renewable energy is sufficient to meet several times the present world energy demand [1]. The hydrogen economy has been identified as one of the most attractive replacement alternatives for the current fossil fuel-based energy system. Not only is hydrogen an environmentally clean energy resource, it is a flexible energy carrier that can convert energy from primary energy sources to different end-user energy forms, such as electricity, heat, and chemicals [2].

Among various renewable forms, wind energy conversion system (WECS) deployment is in an astonishingly rapid expansion, whether onshore or offshore, given the economic advantages of abundant wind power and the increased competitiveness regarding other sources of electric energy [3]. Nowadays, doubly-fed induction generator (DFIG) is the most

* *Corresponding author.*
E-mail address: taoyu1@scut.edu.cn (T. Yu).
http://dx.doi.org/10.1016/j.ijhydene.2017.06.222
0360-3199/

commonly employed generator for wind turbines due to its elegant merits of variable-speed-constant-frequency-based operation, decoupled control of active/reactive power, and partial-scale converters [4]. Normally, a major task of DFIG is to extract the mechanical power from the highly stochastic wind energy as much as possible, which is well-known as maximum power point tracking (MPPT) [5]. Besides, as the stator of DFIG is directly connected to the power grid, it is extremely vulnerable to the grid disturbances, especially grid faults. Hence, proper control strategy needs to be designed to ensure that DFIG is capable of remaining connected to the power grid during the grid faults, also called as low-voltage ride-through (LVRT) [6].

At the moment, vector control (VC) associated with proportional-integral-derivative (PID) control loops is the most popular and widely applied framework in industry, thanks to its unique advantages of decoupled control of active/reactive power, simple structure, as well as high reliability [7]. However, one obvious shortcoming of PID control is that its parameters are determined by one-point linearization of the original nonlinear system, thus the pre-desired control performance might be degraded or even failed when significant variations of operation conditions emerge. Such inherent disadvantage grows much severer for DFIG as it is a highly nonlinear system due to the wind turbine aerodynamics and often operates in various conditions resulted from the stochastic wind speed variation. An enormous variety of metaheuristic optimization techniques have been reported for optimal parameter tuning, e.g., a grouped grey wolf optimizer (GGWO) was proposed to optimize PI control parameters of DFIG for MPPT under different scenarios [8]. Moreover, the gains of PI controller in torque and voltage control loop of rotor-side converter (RSC) are optimized by particle swarm optimization (PSO) to improve the dynamic performance of DFIG by Ref. [9]. Additionally, reference [10] presented a genetic algorithm (GA) to regulate the active and reactive power of DFIG and hence extract maximum energy from the system under varying wind speeds. In work [11], a differential evolutionary algorithm (DE) was proposed to improve the DFIG performance during disturbance through tuning the PI controller parameters. Besides, teaching-learning based optimization (TLBO) was adopted to tune the parameters PI controller of DFIG, which can minimize the damping phenomena, oscillation in rotor currents and fluctuation in electromagnetic torque under various operation conditions [12]. Generally speaking, these algorithms essentially emulate the behaviour of animals/humans who have evolved millions of years of struggle for existence in harshly wild environment. Therefore, they are usually quite powerful to tackle complex real-life management and engineering problems.

Alternatively, plenty of nonlinear robust control schemes have been investigated that aim to remedy the aforementioned thorny problem. For instance, a feedback linearization control (FLC) was designed for MPPT of DFIG with a thorough modal analysis of generator dynamics [13]. Besides, an on-off control scheme based on particle swarm optimization of DFIG was examined by Ref. [14], which superposed the tracking of the optimal torque value. Furthermore, a robust continuous-time model predictive direct power control of DFIG was proposed via Taylor series expansion for stator current prediction, which is directly adopted to compute the required rotor voltage in order to minimize the difference between the actual stator currents and their references over the prediction period [15]. Moreover, an internal model state-feedback approach was examined in Ref. [16] so as to provide great robustness to external disturbances automatically and to eliminate the need of disturbance compensation. Meanwhile, literature [17] reported a multivariable 2-sliding mode control (SMC) for MPPT and robustness enhancement of DFIG, in which unknown nonlinear disturbances and parameter uncertainties are estimated via a fractional-order uncertainty estimator, while a continuous control strategy is developed to realize a chattering-free manner. Additionally, reference [18] described a passive control scheme of DFIG via power shaping for LVRT improvement. Further, a nonlinear active disturbance rejection control (NADRC) was devised to greatly suppress the peak values of stator and rotor currents and DC-link voltage, and to dramatically decrease the oscillation time of electromagnetic torque with only one parameter tuning [19]. In work [20], an approximate dynamics programming (ADP) was presented for the supplementary reactive power control of DFIG. In general, these advanced approaches perform better than linear control but also have a more complex structure, thus their practical implementation might be limited.

Motivated by the above discussions, a natural question can be directly raised: Is there any trade-off proposal that could wisely exploit the noticeable advantages of both linear control and nonlinear robust control, while reduce the malignant effect resulted from their inherent flaws as much as possible? This paper attempts to handle such difficult challenge by designing a perturbation estimation based robust state feedback control (PER-SFC) of DFIG for MPPT. More specifically, the combinatorial effect of wind turbine nonlinearities, generator modelling uncertainties, and wind speed randomness is simultaneously estimated online by a sliding-mode state and perturbation observer (SMSPO), which is then fully compensated by a conventional linear state feedback controller as a supplementary control component. As a consequence, PER-SFC owns the promising features of structure simplicity and high reliability of linear control, as well as global control consistency and significant robustness of nonlinear robust control. In addition, it does not require an accurate DFIG model while only the measurement of rotor speed and reactive power is needed. Four case studies have been undertaken to evaluate the effectiveness of the proposed approach and compare its control performance against to that of other typical methods, such as VC and SMC.

The remaining of this paper is organized as follows: Section DFIG Modelling is devoted for DFIG modelling while Section Perturbation estimation based robust state feedback control develops the PER-SFC scheme. In Section PER-SFC design of DFIG for MPPT, the PER-SFC design of DFIG for MPPT is elaborated in details. Section Case studies provides the simulation results. Finally, Section Conclusions concludes the whole paper.

DFIG modelling

A schematic diagram of DFIG connected to an infinite power grid bus is clearly illustrated by Fig. 1, in which the wind

Please cite this article in press as: Yang B, et al., Perturbation estimation based robust state feedback control for grid connected DFIG wind energy conversion system, International Journal of Hydrogen Energy (2017), http://dx.doi.org/10.1016/j.ijhydene.2017.06.222

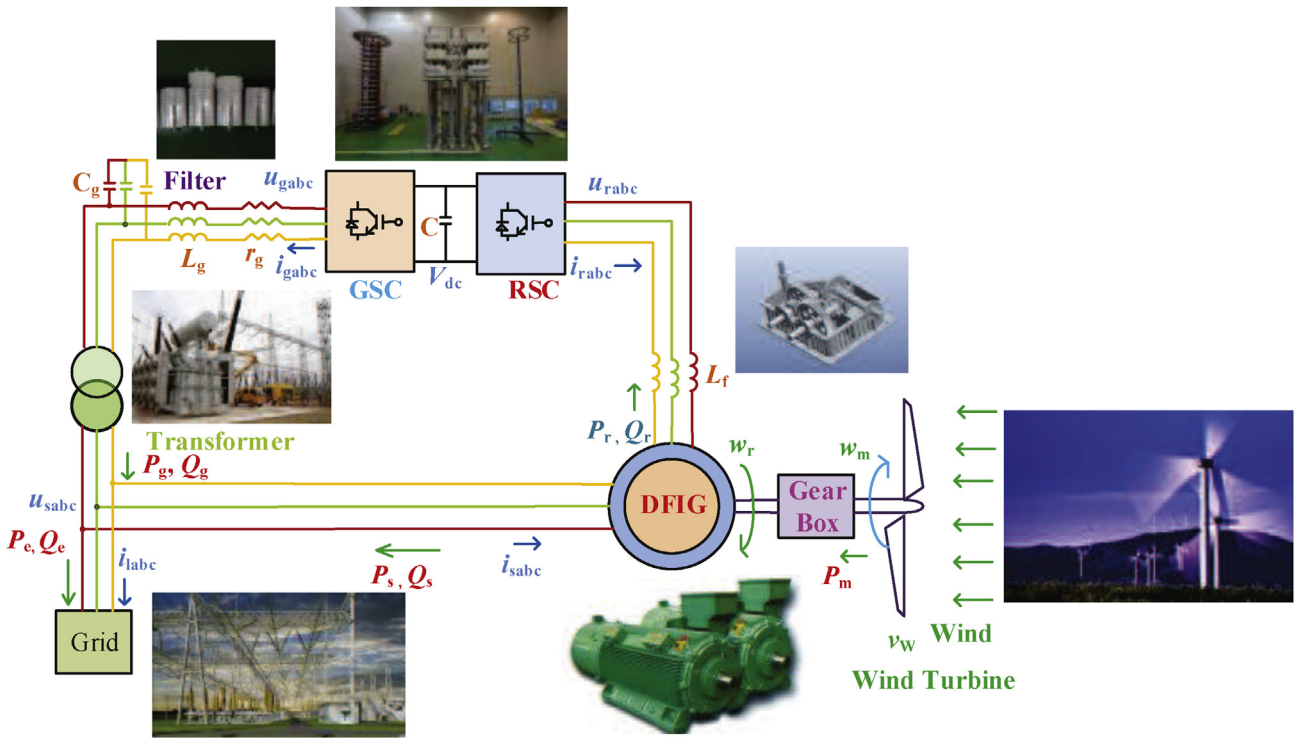

Fig. 1 – The configuration of a DFIG connected to the power grid.

turbine is connected to an induction generator via a lumped mechanical shaft system. Meanwhile, the stator of DFIG is directly connected to the infinite power grid while the rotor of DFIG is fed through a back-to-back converter, respectively.

Wind turbine modelling

In general, the aerodynamics of wind turbine is normally described by a power coefficient $C_p(\lambda,\beta)$, which is usually an algebraic function of both blade pitch angle β and tip-speed-ratio λ, with λ being defined as follows

$$\lambda = \frac{w_m R}{v_{wind}} \tag{1}$$

where ω_m denotes the wind turbine rotational speed and v_{wind} represents the wind speed; R is the radius of wind turbine blade. According to the wind turbine dynamics, a generic equation employed to describe the power coefficient $C_p(\lambda,\beta)$ can be written as

$$C_p(\lambda,\beta) = c_1\left(\frac{c_2}{\lambda_i} - c_3\beta - c_4\right)e^{-\frac{c_5}{\lambda_i}} + c_6\lambda \tag{2}$$

with

$$\frac{1}{\lambda_i} = \frac{1}{\lambda + 0.08\beta} - \frac{0.035}{\beta^3 + 1} \tag{3}$$

The coefficients c_1 to c_6 are selected as $c_1 = 0.5176$, $c_2 = 116$, $c_3 = 0.4$, $c_4 = 5$, $c_5 = 21$ and $c_6 = 0.0068$, respectively [8].

Besides, the mechanical power extracted by the wind turbine from the wind energy can be calculated by

$$P_m = \frac{1}{2}\rho\pi R^2 C_p(\lambda,\beta)v_{wind}^3 \tag{4}$$

where ρ is the air density. Note that this paper focuses on the MPPT of DFIG, hence the wind turbine merely operates in the sub-rated speed range while its pitch control is deactivated, e.g., $\beta\equiv 0$ for the whole operation of DFIG.

Doubly-fed induction generator modelling

The generator dynamics can be written as [8,13]:

$$\frac{di_{qs}}{dt} = \frac{\omega_b}{L_s'}\left(-R_1 i_{qs} + \omega_s L_s' i_{ds} + \frac{\omega_r}{\omega_s}e_{qs}' - \frac{1}{T_r\omega_s}e_{ds}' - v_{qs} + \frac{L_m}{L_{rr}}v_{qr}\right) \tag{5}$$

$$\frac{di_{ds}}{dt} = \frac{\omega_b}{L_s'}\left(-\omega_s L_s' i_{qs} - R_1 i_{ds} + \frac{1}{T_r\omega_s}e_{qs}' + \frac{\omega_r}{\omega_s}e_{ds}' - v_{ds} + \frac{L_m}{L_{rr}}v_{dr}\right) \tag{6}$$

$$\frac{de_{qs}'}{dt} = \omega_b\omega_s\left[R_2 i_{ds} - \frac{1}{T_r\omega_s}e_{qs}' + \left(1 - \frac{\omega_r}{\omega_s}\right)e_{ds}' - \frac{L_m}{L_{rr}}v_{dr}\right] \tag{7}$$

$$\frac{de_{ds}'}{dt} = \omega_b\omega_s\left[-R_2 i_{qs} - \left(1 - \frac{\omega_r}{\omega_s}\right)e_{qs}' - \frac{1}{T_r\omega_s}e_{ds}' + \frac{L_m}{L_{rr}}v_{qr}\right] \tag{8}$$

where ω_b denotes the electrical base speed while ω_s is the synchronous angular speed; e_{ds}' and e_{qs}' are the equivalent d-axis and q-axis (dq-) internal voltages of the generator; i_{ds} and i_{qs} are the dq-stator currents of the generator; v_{ds} and v_{qs} represent the dq-stator terminal voltages of the generator; Lastly, v_{dr} and v_{qr} are the dq-rotor voltages of the generator. The remaining parameters and symbols could be referred to literature [25].

In addition, the active power P_e produced by the DFIG is calculated by

$$P_e = e_{qs}' i_{qs} + e_{ds}' i_{ds} \tag{9}$$

Please cite this article in press as: Yang B, et al., Perturbation estimation based robust state feedback control for grid connected DFIG wind energy conversion system, International Journal of Hydrogen Energy (2017), http://dx.doi.org/10.1016/j.ijhydene.2017.06.222

Here, the q-axis is aligned with the stator voltage thus the d-axis leads the q-axis. Under such framework, it can be readily obtain that $v_{ds}\equiv 0$ and v_{qs} equals to the magnitude of the terminal voltage. At last, the reactive power Q_s is generated as

$$Q_s = v_{qs}i_{ds} - v_{ds}i_{qs} = v_{qs}i_{ds} \tag{10}$$

It is worth noting that the power losses produced in the rotor are ignored.

Mechanical shaft system modelling

A single lumped-mass shaft system whose lumped inertia constant is denoted by H_m is adopted to model the mechanical shaft system of DFIG, which yields [24].

$$H_m = H_t + H_g \tag{11}$$

where H_g and H_t are the inertia constants of the generator and wind turbine, respectively.

Furthermore, one can write the electromechanical dynamics as

$$\frac{d\omega_m}{dt} = \frac{1}{2H_m}(T_m - T_e - D\omega_m) \tag{12}$$

where ω_m is the rotational speed of the mechanical lumped-mass system that equals to the generator rotor speed ω_r when both of them are given in per unit (p.u.); D denotes the damping constant of the mechanical lumped-mass system; and T_m represents the mechanical torque which can be directly calculated by $T_m = P_m/\omega_m$.

Note that only the dynamics of RSC is considered while the dynamics of grid-side converter (GSC) is ignored, as the former one attempts to track the wind power and the latter one focuses on the DC voltage maintenance.

Perturbation estimation based robust state feedback control

Consider a nonlinear uncertain system which has the following canonical form

$$\begin{cases} \dot{x} = Ax + B(a(x) + b(x)u + d(t)) \\ y = x_1 \end{cases} \tag{13}$$

where $x = [x_1, x_2, \cdots, x_n]^T \in \mathbb{R}^n$ is the state variable vector; $u \in \mathbb{R}$ and $y \in \mathbb{R}$ are the control input and system output, respectively; $a(x) : \mathbb{R}^n \mapsto \mathbb{R}$ and $b(x) : \mathbb{R}^n \mapsto \mathbb{R}$ are unknown smooth functions; and $d(t) : \mathbb{R}^+ \mapsto \mathbb{R}$ represents a time-varying external disturbance. The $n \times n$ matrix A and $n \times 1$ matrix B are of the canonical form as follows

$$A = \begin{bmatrix} 0 & 1 & 0 & \cdots & 0 \\ 0 & 0 & 1 & \cdots & 0 \\ \vdots & & & & \vdots \\ 0 & 0 & 0 & \cdots & 1 \\ 0 & 0 & 0 & \cdots & 0 \end{bmatrix}_{n\times n}, B = \begin{bmatrix} 0 \\ 0 \\ \vdots \\ 0 \\ 1 \end{bmatrix}_{n\times 1} \tag{14}$$

The perturbation of system (13) is defined as [21].

$$\Psi(x, u, t) = a(x) + (b(x) - b_0)u + d(t) \tag{15}$$

where b_0 is the constant control gain.

From the original system (13), the last state x_n can be rewritten in the presence of perturbation (15), gives

$$\dot{x}_n = a(x) + (b(x) - b_0)u + d(t) + b_0u = \Psi(x, u, t) + b_0u \tag{16}$$

Define an extended state $x_{n+1} = \Psi(x, u, t)$. Then, system (13) can be directly extended into

$$\begin{cases} y = x_1 \\ \dot{x}_1 = x_2 \\ \vdots \\ \dot{x}_n = x_{n+1} + b_0u \\ \dot{x}_{n+1} = \dot{\Psi}(\cdot) \end{cases} \tag{17}$$

The new state vector becomes $x_e = [x_1, x_2, \cdots, x_n, x_{n+1}]^T$, and the following three assumptions are made.

- A.1 b_0 is chosen to satisfy: $|b(x)/b_0 - 1| \le \theta < 1$, where θ is a positive constant.
- A.2 The functions $\Psi(x, u, t) : \mathbb{R}^n \times \mathbb{R} \times \mathbb{R}^+ \mapsto \mathbb{R}$ and $\dot{\Psi}(x, u, t) : \mathbb{R}^n \times \mathbb{R} \times \mathbb{R}^+ \mapsto \mathbb{R}$ are bounded over the domain of interest: $|\Psi(x, u, t)| \le \gamma_1$, $|\dot{\Psi}(x, u, t)| \le \gamma_2$ with $\Psi(0, 0, 0) = 0$ and $\dot{\Psi}(0, 0, 0) = 0$, where γ_1 and γ_2 are positive constants.

Throughout this paper, $\tilde{x} = x - \hat{x}$ refers to the estimation error of x whereas $\hat{x}$ represents the estimate of x, while x^* represents the reference of x. In the consideration of the worst case, e.g., $y = x_1$ is the only measurable state, an $(n+1)$th-order SMSPO for the extended system (17) is designed to simultaneously estimate the system states and perturbation, shown as follows

$$\begin{cases} \dot{\hat{x}}_1 = \hat{x}_2 + \alpha_1\tilde{x}_1 + k_1 \mathrm{sat}(\tilde{x}_1, \varepsilon_o) \\ \vdots \\ \dot{\hat{x}}_n = \hat{\Psi}(\cdot) + \alpha_n\tilde{x}_1 + k_n \mathrm{sat}(\tilde{x}_1, \varepsilon_o) + b_0u \\ \dot{\hat{\Psi}}(\cdot) = \alpha_{n+1}\tilde{x}_1 + k_{n+1}\mathrm{sat}(\tilde{x}_1, \varepsilon_o) \end{cases} \tag{18}$$

where α_i, $i = 1, 2, \cdots, n+1$, are the Luenberger observer constants which are chosen to place the poles of $s^{n+1} + \alpha_1 s^n + \alpha_2 s^{n-1} + \cdots + \alpha_{n+1} = (s + \lambda_\alpha)^{n+1} = 0$ being in the open left-half complex plane at $-\lambda_\alpha$, with $\alpha_i = C_{n+1}^i \lambda_\alpha^i$, $i = 1, 2, \cdots, n+1$. In addition, positive constants k_i are the sliding surface constants, in which $k_1 \ge |\tilde{x}_2|^{max}$, where the ratio $k_i/k_1 (i = 2, 3, \cdots, n+1)$ be chosen to put the poles of $p^n + (k_2/k_1)p^{n-1} + \cdots + (k_n/k_1)p + (k_{n+1}/k_1) = (p + \lambda_k)^n = 0$ to be in the open left-half complex plane at $-\lambda_k$. It has $k_{i+1} = C_n^i \lambda_k^i k_1$, $i = 1, 2, \cdots, n$. Moreover, $\mathrm{sat}(\tilde{x}_1, \varepsilon_o)$ function is employed to replace conventional $\mathrm{sgn}(\tilde{x}_1)$ function, such that the malignant effect of chattering in SMSPO resulted from discontinuity can be reduced, which is defined as $\mathrm{sat}(\tilde{x}_1, \varepsilon_o) = \tilde{x}_1/|\tilde{x}_1|$ when $|\tilde{x}_1| > \varepsilon_o$ and $\mathrm{sat}(\tilde{x}_1, \varepsilon_o) = \tilde{x}_1/\varepsilon_o$ when $|\tilde{x}_1| \le \varepsilon_o$. Lastly, ε_o denotes the observer thickness layer boundary.

The PER-SFC for system (13) can be designed as

$$u = \frac{1}{b_0}\left[x_1^{*(n)} - \hat{\Psi}(\cdot) + K_P(\hat{x}_1 - x_1^*) + K_I\int(\hat{x}_1 - x_1^*) + K_D\frac{d}{dt}(\hat{x}_1 - x_1^*)\right] \tag{19}$$

Please cite this article in press as: Yang B, et al., Perturbation estimation based robust state feedback control for grid connected DFIG wind energy conversion system, International Journal of Hydrogen Energy (2017), http://dx.doi.org/10.1016/j.ijhydene.2017.06.222

where perturbation estimate $\widehat{\Psi}(\cdot)$ is used to globally remove the system nonlinearities and uncertainties, such that a consistent control performance under various operation conditions can be achieved. Therefore, the inherent weakness of linear control can be considerably reduced. Here, proportional gain K_P, integral gain K_I, and derivative gain K_D can be equivalently treated as PID loop gains.

PER-SFC design of DFIG for MPPT

Choose the tracking error $e = [e_1 \ e_2]^T$ of rotor speed ω_r and stator reactive power Q_s as the outputs, yields

$$\begin{cases} e_1 = \omega_r - \omega_r^* \\ e_2 = Q_s - Q_s^* \end{cases} \tag{20}$$

where rotor speed reference $\omega_r^* = \lambda_{opt} v_{wind}/R$ and Q_s^* denotes the reactive power reference. Differentiate tracking error (20) until the control inputs v_{dr} and v_{qr} appeared explicitly, it obtains

$$\begin{bmatrix} \ddot{e}_1 \\ \dot{e}_2 \end{bmatrix} = \begin{bmatrix} f_1 & - & \ddot{\omega}_r^* \\ f_2 & - & \dot{Q}_s^* \end{bmatrix} + B \begin{bmatrix} v_{dr} \\ v_{qr} \end{bmatrix} \tag{21}$$

where

$$f_1 = \frac{\dot{T}_m}{2H_m} - \frac{1}{2H_m}\left\{ w_b \left[\left(1 - \frac{\omega_r}{\omega_s}\right)\left(e'_{ds} i_{qs} - e'_{qs} i_{ds}\right) - \frac{1}{\omega_s T_r}\left(e'_{qs} i_{qs} + e'_{ds} i_{ds}\right)\right] + \frac{\omega_b}{\omega_s L'_s}\left[\frac{\omega_r}{\omega_s}\left(e'^2_{ds} + e'^2_{qs}\right) + \omega_s L'_s\left(e'_{qs} i_{ds} - e'_{ds} i_{qs}\right) - R_1\left(e'_{qs} i_{qs} + e'_{ds} i_{ds}\right) - e'_{qs} v_{qs} - e'_{ds} v_{ds}\right]\right\} \tag{22}$$

$$\begin{bmatrix} v_{dr} \\ v_{qr} \end{bmatrix} = B_0^{-1}\left[\ddot{\omega}_r^* - \widehat{\Psi}_1(\cdot) + K_{P1}(\widehat{\omega}_r - \omega_r^*) + K_{I1}\int(\widehat{\omega}_r - \omega_r^*) + K_{D1}\frac{d}{dt}(\widehat{\omega}_r - \omega_r^*)\right.$$
$$\left.\dot{Q}_s^* - \widehat{\Psi}_2(\cdot) + K_{P2}(\widehat{Q}_s - Q_s^*) + K_{I2}\int(\widehat{Q}_s - Q_s^*) + K_{D2}\frac{d}{dt}(\widehat{Q}_s - Q_s^*)\right]$$

$$f_2 = \frac{\omega_b}{L'_s}\left(\omega_s L'_s i_{qs} + R_1 i_{ds} - \frac{1}{\omega_s T_r} e'_{qs} - \frac{\omega_r}{\omega_s} e'_{ds}\right) v_{qs} + \frac{\omega_b}{L'_s}\left(- R_1 i_{qs} + \omega_s L'_s i_{ds} + \frac{\omega_r}{\omega_s} e'_{qs} - \frac{1}{\omega_s T_r} e'_{ds} - v_{qs}\right) v_{ds} \tag{23}$$

and

$$B = \begin{bmatrix} \frac{\omega_b L_m}{-2H_m L_{rr}}\left(\frac{e'_{ds}}{\omega_s L'_s} - i_{qs}\right) & \frac{\omega_b L_m}{-2H_m L_{rr}}\left(\frac{e'_{qs}}{\omega_s L'_s} + i_{ds}\right) \\ -\frac{\omega_b L_m}{L'_s L_{rr}} v_{qs} & \frac{\omega_b L_m}{L'_s L_{rr}} v_{ds} \end{bmatrix} \tag{24}$$

where B is called the control gain matrix. As $\det(B) = -\frac{\omega_b^2 L_m^2 v_{qs}}{2H_m L'_s L_{rr}^2}\left(\frac{e'_{qs}}{\omega_s L_s} + i_{ds}\right) \neq 0$, hence it is invertible while the transformed system is linearizable over the whole operation range of DFIG.

Assume all the nonlinearities are unknown, define the perturbations $\Psi_1(\cdot)$ and $\Psi_2(\cdot)$ for system (21) as

$$\begin{bmatrix} \Psi_1(\cdot) \\ \Psi_2(\cdot) \end{bmatrix} = \begin{bmatrix} f_1 \\ f_2 \end{bmatrix} + (B - B_0)\begin{bmatrix} v_{dr} \\ v_{qr} \end{bmatrix} \tag{25}$$

where the constant control gain B_0 is given by

$$B_0 = \begin{bmatrix} b_{11} & 0 \\ 0 & b_{22} \end{bmatrix} \tag{26}$$

Then system (21) can be rewritten as

$$\begin{bmatrix} \ddot{e}_1 \\ \dot{e}_2 \end{bmatrix} = \begin{bmatrix} \Psi_1(\cdot) \\ \Psi_2(\cdot) \end{bmatrix} + B_0 \begin{bmatrix} v_{dr} \\ v_{qr} \end{bmatrix} - \begin{bmatrix} \ddot{\omega}_r^* \\ \dot{Q}_s^* \end{bmatrix} \tag{27}$$

Define $z_{11} = \omega_r$ and $z_{12} = \dot{z}_{11}$, a third-order SMSPO is adopted to estimate $\Psi_1(\cdot)$ as

$$\begin{cases} \dot{\hat{z}}_{11} = \hat{z}_{12} + \alpha_{11}\tilde{\omega}_r + k_{11} sat(\tilde{\omega}_r, \varepsilon_o) \\ \dot{\hat{z}}_{12} = \hat{\Psi}_1(\cdot) + \alpha_{12}\tilde{\omega}_r + k_{12} sat(\tilde{\omega}_r, \varepsilon_o) + b_{11} v_{dr} \\ \dot{\hat{\Psi}}_1(\cdot) = \alpha_{13}\tilde{\omega}_r + k_{13} sat(\tilde{\omega}_r, \varepsilon_o) \end{cases} \tag{28}$$

where observer gains k_{11}, k_{12}, k_{13}, α_{11}, α_{12}, and α_{13}, are all positive constants.

Define $z_{21} = Q_s$, a second-order sliding-mode perturbation observer (SMPO) is employed to estimate $\Psi_2(\cdot)$ as

$$\begin{cases} \dot{\hat{z}}_{21} = \hat{\Psi}_2(\cdot) + \alpha_{21}\tilde{Q}_s + k_{21} sat\left(\tilde{Q}_s, \varepsilon_o\right) + b_{22} v_{qr} \\ \dot{\hat{\Psi}}_2(\cdot) = \alpha_{22}\tilde{Q}_s + k_{22} sat\left(\tilde{Q}_s, \varepsilon_o\right) \end{cases} \tag{29}$$

where observer gains k_{21}, k_{22}, α_{21}, and α_{22}, are all positive constants.

The PER-SFC law for system (21) is designed as

where linear state feedback control gains K_{Pi}, K_{Ii}, K_{Di}, $i = 1, 2$, determine the closed-loop dynamics.

During the most severe disturbance, both the rotor speed and reactive power may reduce from their initial value to around zero within a short period of time Δ. Thus the boundary values of the system state and perturbation estimates can be calculated by $|\hat{z}_{11}| \leq |\omega_r^*|$, $|\hat{z}_{12}| \leq |\omega_r^*|/\Delta$, and $|\widehat{\Psi}_1(\cdot)| \leq |\omega_r^*|/\Delta^2$, $|\hat{z}_{21}| \leq |Q_s^*|$, and $|\widehat{\Psi}_2(\cdot)| \leq |Q_s^*|/\Delta$, respectively. Note that the selection of B_0 (26) fully decouples system (21) into two single-input single-output (SISO) systems (27). As a result, control inputs v_{dr} and v_{qr} can independently regulate rotor speed ω_r and reactive power Q_s.

To this end, the overall PER-SFC structure of DFIG for MPPT is illustrated by Fig. 2, in which only the measurement of rotor speed ω_r and reactive power Q_s at the RSC side is required. At

Please cite this article in press as: Yang B, et al., Perturbation estimation based robust state feedback control for grid connected DFIG wind energy conversion system, International Journal of Hydrogen Energy (2017), http://dx.doi.org/10.1016/j.ijhydene.2017.06.222

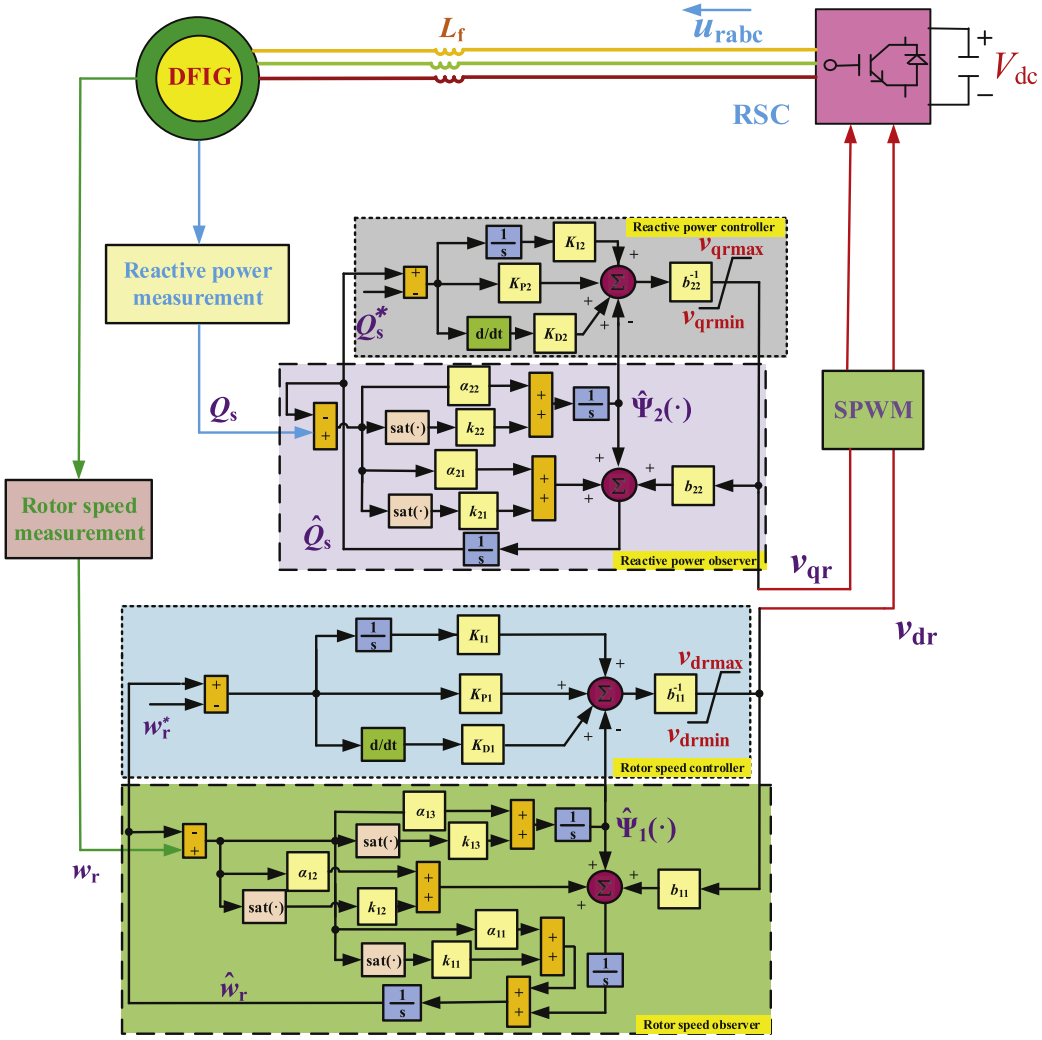

Fig. 2 – The overall PER-SFC structure of DFIG for MPPT.

last, the obtained control inputs (30) are modulated by the sinusoidal pulse width modulation (SPWM) technique [26].

Case studies

The proposed PER-SFC is employed for MPPT of a DFIG connected to the power grid, which control performance is compared to that of conventional vector control (VC) [7] and sliding-mode control (SMC) [27], under four scenarios, i.e., step change of wind speed, random wind speed variation, LVRT, and robustness against parameter uncertainties. Consider the control inputs might exceed the admissible capacity of RSC at some operation point, hence their values must be limited. Here, υ_{dr} and υ_{qr} are scaled proportionally as: if $\upsilon_r = \sqrt{\upsilon_{dr}^2 + \upsilon_{qr}^2} > \upsilon_r^{max}$, then set $\upsilon_{dr}^{lim} = \upsilon_{dr}\upsilon_r^{max}/\upsilon_r$ and $\upsilon_{qr}^{lim} = \upsilon_{qr}\upsilon_r^{max}/\upsilon_r$ [13], respectively.

Moreover, the PER-SFC parameters are tabulated in Table 1. Here, observer gains of SMSPO and SMPO are chosen to be $\lambda_{\alpha 1} = 10$ and $\lambda_{\alpha 2} = 20$, together with the sliding surface constants $\lambda_{k1} = 10$ and $\lambda_{k2} = 40$, respectively, which ensures a proper trade-off between the estimation convergence rate and estimation error, i.e., larger observer gains usually result in a faster estimation convergence rate and higher estimation error, vice versa. Normally an observer gain ranging between 10 and 50 can satisfy most of the cases [29]. Through trial-and-error, this paper chooses these observer gains and the PID control parameters to guarantee a satisfactory control performance and observer estimation performance.

Table 1 – PER-SFC parameters for DFIG.

rotor controller gains			
$b_{11} = -5000$	$K_{P1} = -1500$	$K_{I1} = -1000$	$K_{D1} = -200$
rotor observer gains			
$\alpha_{11} = 30$	$\alpha_{12} = 300$	$\alpha_{13} = 1000$	$\varepsilon_o = 0.2$
$k_{11} = 20$	$k_{12} = 600$	$k_{13} = 6000$	
reactive power controller gains			
$b_{22} = -2000$	$K_{P2} = -800$	$K_{I2} = -500$	$K_{D2} = -80$
reactive power observer gains			
$\alpha_{21} = 40$	$\alpha_{22} = 400$	$k_{21} = 15$	$k_{22} = 600$

Please cite this article in press as: Yang B, et al., Perturbation estimation based robust state feedback control for grid connected DFIG wind energy conversion system, International Journal of Hydrogen Energy (2017), http://dx.doi.org/10.1016/j.ijhydene.2017.06.222

The simulation is executed on Matlab/Simulink 7.10 using a personal computer with an IntelR CoreTMi7 CPU at 2.2 GHz and 4 GB of RAM. Note that all the produced active power will be fully absorbed by the infinite power grid which is usually treated as an ideal electrical load, such assumption is quite common and general in the design of MPPT of DFIG [8,13,16,25]. Hence, such ideal electrical load is used in all the following simulations.

Step change of wind speed

A series of three consecutive step changes of wind speed are applied to briefly mimic a gust, i.e., 8–9 m/s, 9–11 m/s, 11–12 m/s at t = 5 s, 12.5 s, 20 s, respectively. The MPPT performance of the three controllers is demonstrated in Fig. 3. During such scenario, as the wind speed increases sharply, the mechanical power injected into the DFIG varies rapidly thus a power imbalance is resulted in, which leads to the power oscillations. Then, more electrical power needs to be generated by the DFIG by increasing the control inputs until the power is balanced again. In addition, Fig. 3 clearly shows that PER-SFC can extract the optimal wind power with tiny power oscillations, meanwhile it can also regulate the active power and reactive power more rapidly and smoothly compared to that of VC and SMC. Moreover, VC performance is degraded considerably at different operation points.

Random variation of wind speed

A stochastic wind speed variation is simulated to investigate the control performance of PER-SFC, in which the wind speed starts from 8 m/s and gradually arrives at 12 m/s in 15 s, as illustrated by Fig. 4. The system responses are presented in Fig. 5, from which one can find that PER-SFC could effectively reduce the unfavourable oscillations of rotor speed error and reactive power thanks to the real-time perturbation compensation. Similar to the step change of wind speed, the power oscillation is a direct result from the power imbalance between the mechanical power (wind energy) and electrical power (DFIG). However, as the variation of random wind speed is not as sharp as that of the step change, its peak magnitude of oscillation when the power imbalance occurs is not as significant as that of step change. In addition, its power coefficient is the closest to the optimum point, such that the wind energy can be optimally extracted in the presence of random wind speed variations.

It is worth noting that the active power decreases at first 4 s while the wind speed increases, this is due to the inertia of mechanical shaft system. e.g., when the wind speed increases at a specific moment, the mechanical power is increased immediately. However, the rotor speed cannot increase immediately due to the mechanical shaft inertia, this phenomenon can also be seen from the rotor tracking curve of Fig. 5 that rotor error is decreased at first. The fastest way to

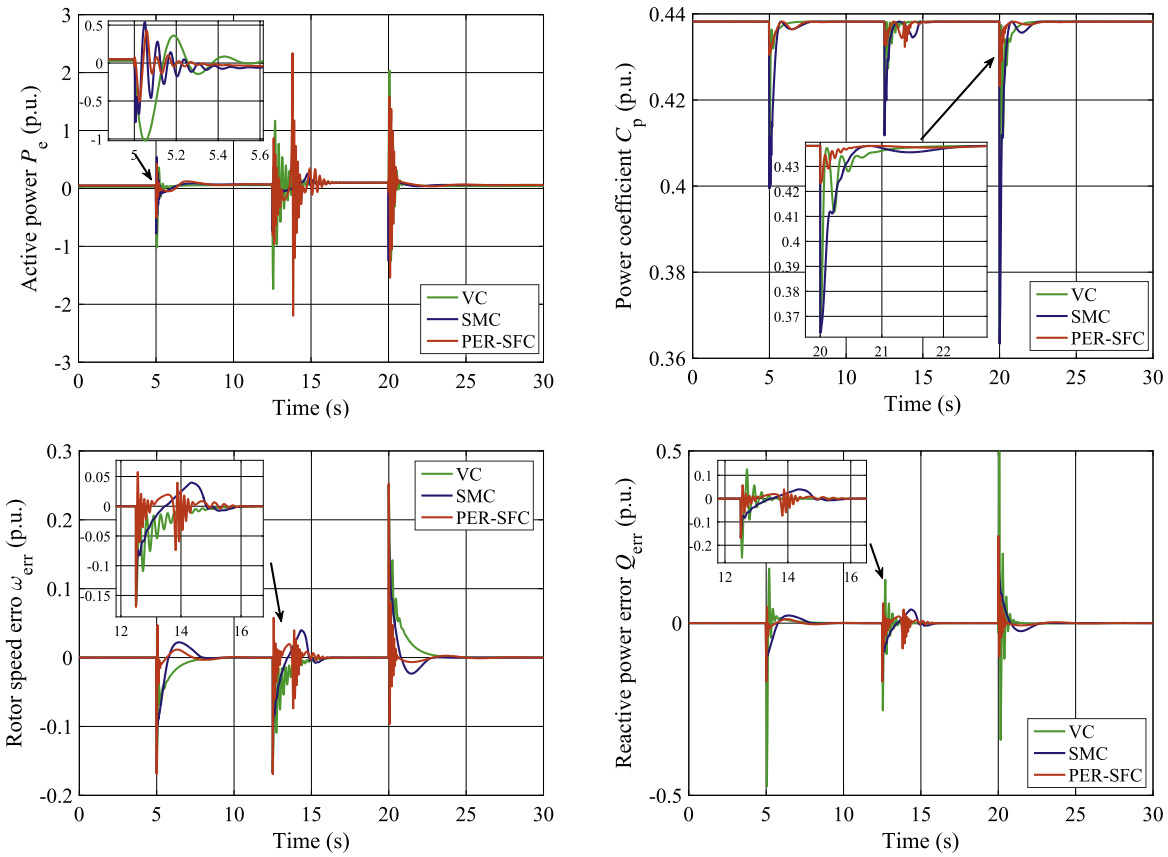

Fig. 3 – Disturbance rejection performance under three consecutive step changes of a wind gust from 8 m/s to 12 m/s.

Please cite this article in press as: Yang B, et al., Perturbation estimation based robust state feedback control for grid connected DFIG wind energy conversion system, International Journal of Hydrogen Energy (2017), http://dx.doi.org/10.1016/j.ijhydene.2017.06.222

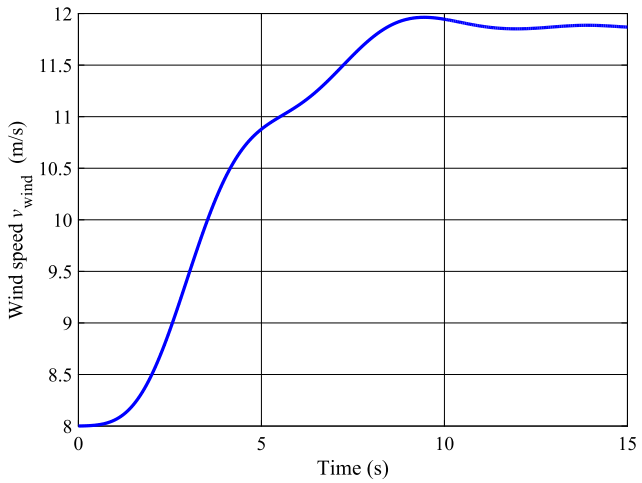

Fig. 4 – The profile of random wind speed varied from 8 m/s to 12 m/s.

handle such inertia effect is to decrease the active power temporarily so the accelerating active power, e.g., $P_a = P_m - P_e$, can grow more significantly, such that a higher accelerating torque could be generated thus the tracking of wind speed can be faster [8]. Note that such phenomenon just emerges during the first several seconds when a sudden wind speed variation occurs as the rotor speed need to be accelerated dramatically. After this period, the rotor speed does not need to respond so rapidly.

LVRT performance

With the rapidly ever-growing integration of WECS into the main power grid, it usually requires WECS to realize LVRT when the power grid voltage is temporarily reduced due to a fault or load change in the power grid, or can even address the generator to stay operational and not disconnect from the power grid during and after the voltage dip [28]. A 625 ms voltage drop starts at $t = 1$ s from nominal value to 0.3 p.u. and restores to 0.9 p.u. is applied, while the DFIG responses are provided by Fig. 6. Unlike the above two cases, the power imbalance caused in LVRT is not due to the variation of mechanical power, but instead, led by the sudden decrease of electrical power from the power grid. As it is impossible to adjust the mechanical power (wind energy is uncontrollable), the DFIG has to respond to increase its output power to alleviate such power oscillation by adjusting its rotor voltage.

Obviously, PER-SFC can effectively damp the reactive power oscillations while extract the maximal wind power during LVRT as it can maintain the power coefficient to be the closest to its optimum. In comparison, VC requires the longest time to restore the disturbed DFIG system from such sudden contingencies. Besides, the control costs of different approaches show that relatively reasonable control costs are

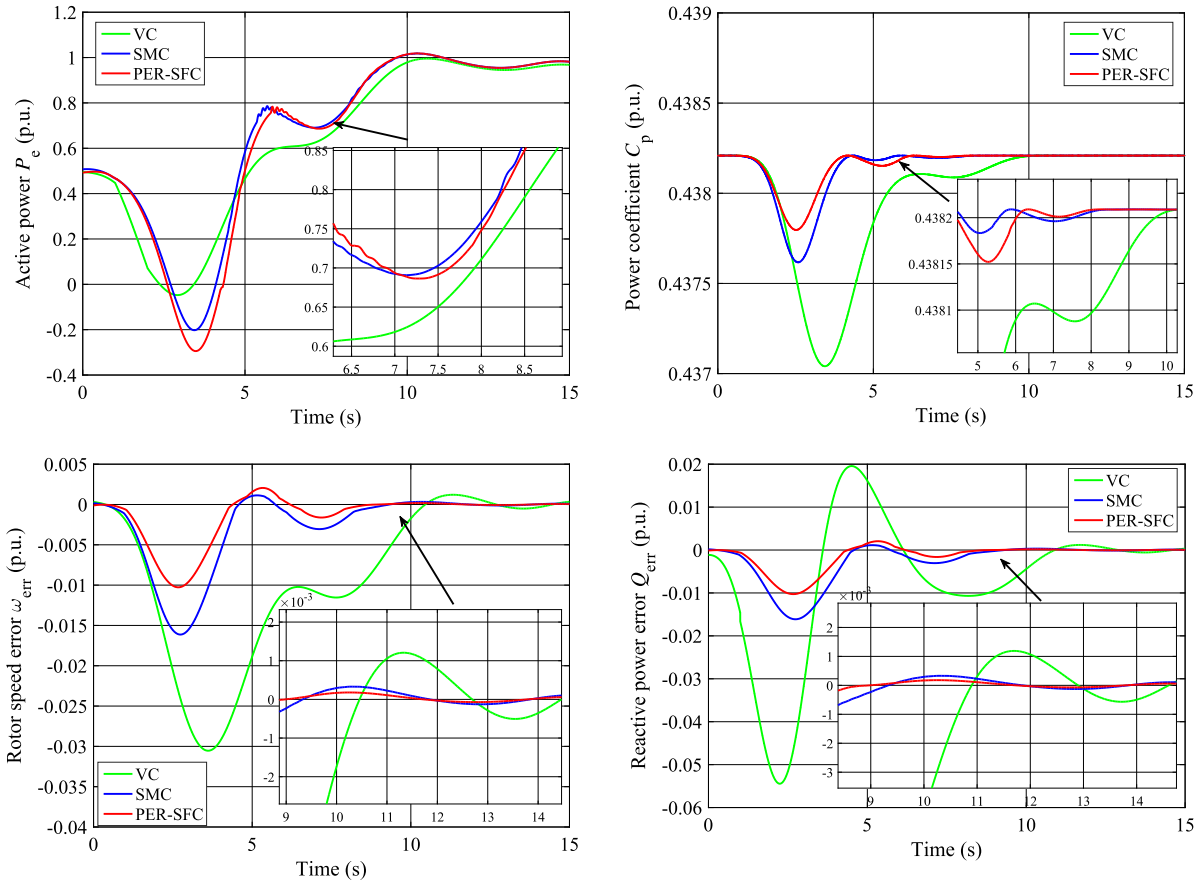

Fig. 5 – MPPT performance to a random variation of wind speed obtained from 8 m/s to 12 m/s.

Please cite this article in press as: Yang B, et al., Perturbation estimation based robust state feedback control for grid connected DFIG wind energy conversion system, International Journal of Hydrogen Energy (2017), http://dx.doi.org/10.1016/j.ijhydene.2017.06.222

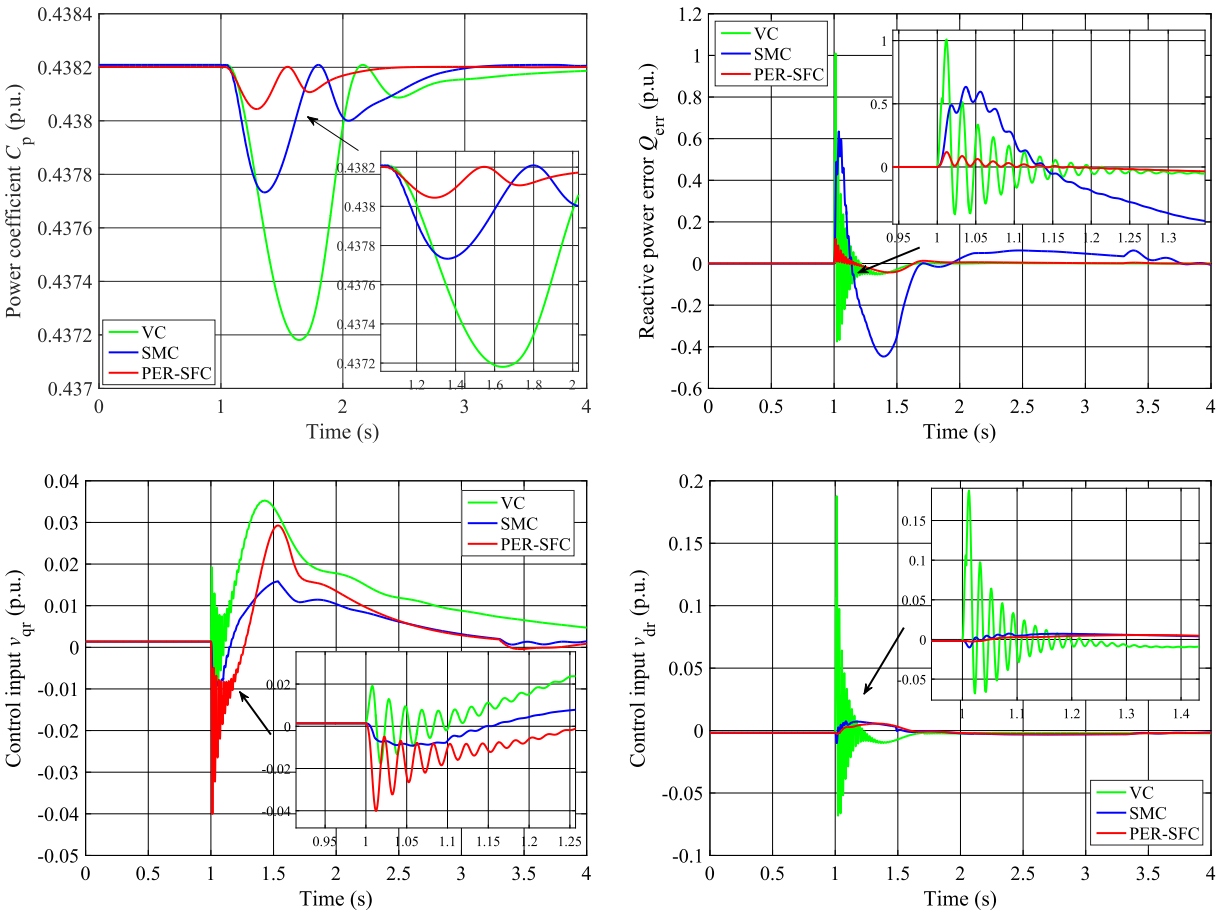

Fig. 6 – DFIG responses obtained under LVRT (a 625 ms voltage dip staring at t = 1 s from nominal value to 0.3 p.u. and restores to 0.9 p.u.).

required by PER-SFC. Finally, the perturbation estimation performance of SMSPO and SMPO has been carefully monitored, as shown in Fig. 7. It gives that the real perturbation is rapidly tracked, such that their effectiveness can be validated.

Robustness against parameter uncertainties

In order to evaluate the robustness against parameter uncertainties, a series of plant-model mismatches of stator resistance R_s and mutual inductance L_m with ±20% variation around their nominal value are undertaken, in which a 0.25 p.u. voltage drop for 0.1 s at power grid is applied. The peak value of active power $|P_e|$ is recorded for a clear comparison. Fig. 8 illustrates that the variation of $|P_e|$ obtained by VC, SMC, PER-SFC is 12.3%, 4.92%, 6.15%, respectively. It is worth noting that SMC has a slightly stronger robustness than that of PER-SFC due to its sliding-mode mechanism. However, the control structure of SMC is quite complex which is also associated

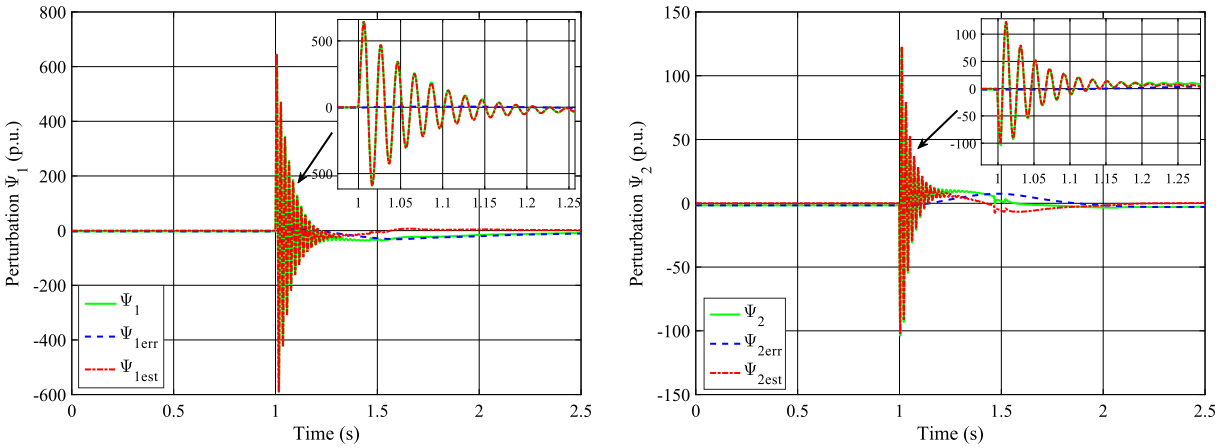

Fig. 7 – Perturbation estimation performance of SMSPO and SMPO obtained during LVRT.

Please cite this article in press as: Yang B, et al., Perturbation estimation based robust state feedback control for grid connected DFIG wind energy conversion system, International Journal of Hydrogen Energy (2017), http://dx.doi.org/10.1016/j.ijhydene.2017.06.222

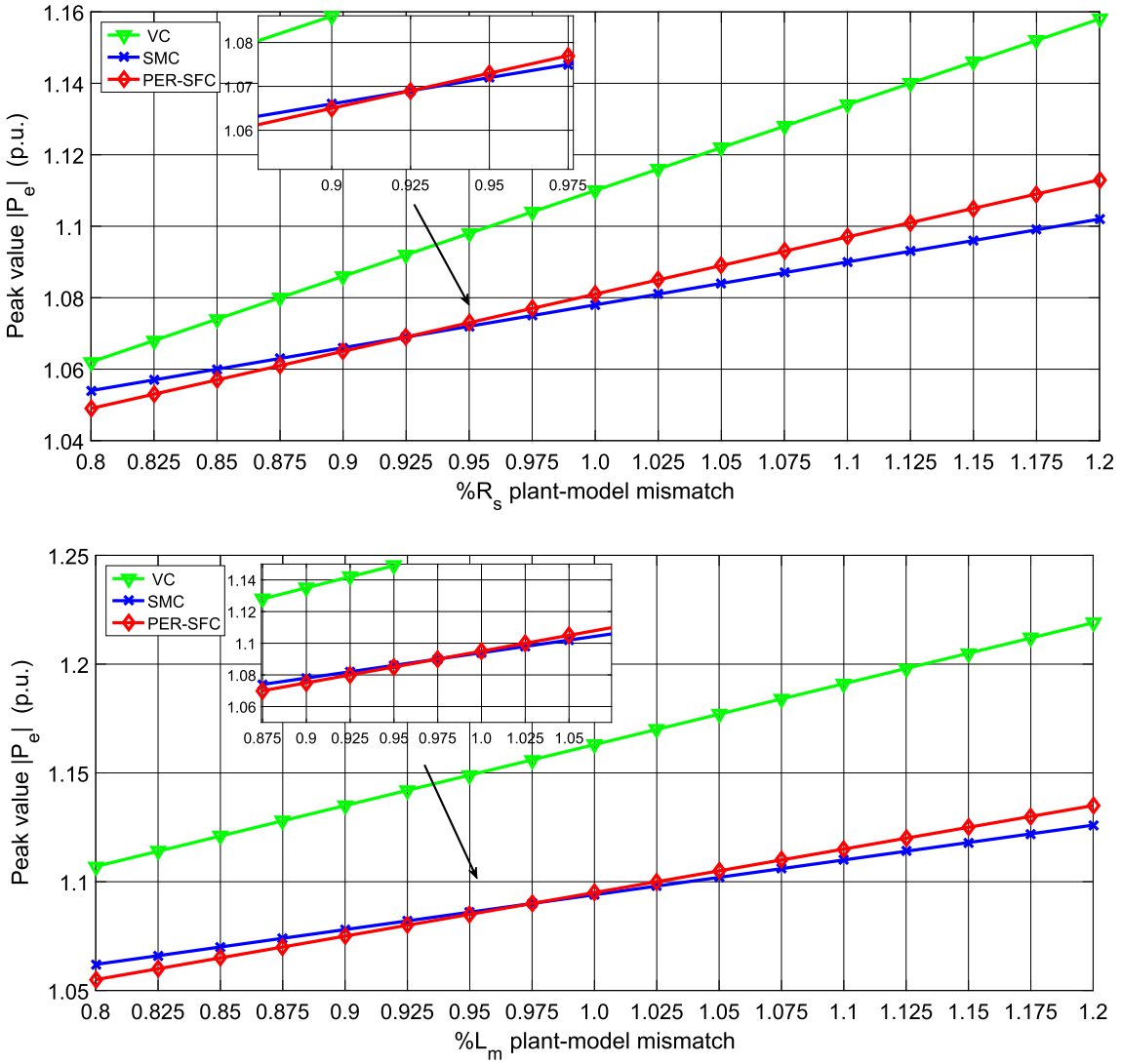

Fig. 8 – Peak value of active power $|P_e|$ obtained under a 0.25 p.u. voltage drop lasting 1 s at power grid with 20% variation of the stator resistance R_s and mutual inductance L_m of different approaches, respectively.

with discontinuity in controller loop, while PER-SFC employs a very simple PID control structure and the discontinuity is merely involved in observer loop.

Comparative studies

The integral of absolute error (IAE) indices of each approach calculated in different cases are summarized in Table 2, where $IAE_x = \int_0^T |x - x^*| dt$ and x^* is the reference of variable x. The simulation time $T = 30$ s. It provides that PER-SFC owns the lowest IAE indices (in bold) in all scenarios among all approaches. In particular, its IAE_Q obtained in LVRT is merely 23.03% and 47.37% to that of VC and SMC, respectively; Besides, its IAE_ω obtained in LVRT is just 25.12% and 49.85% to that of VC and SMC, respectively.

To this end, the overall control costs of three controllers required in three scenarios are compared in Fig. 9. Here, PER-SFC merely needs the lowest control costs in all scenarios due

Table 2 – IAE indices (in p.u.) of different control schemes obtained in different cases.

Method/ Scenario	Step change of wind speed		Random variation of wind speed		Low voltage ride-through	
	IAE_Q	IAE_ω	IAE_Q	IAE_ω	IAE_Q	IAE_ω
VC	1.96E – 02	4.11E – 03	4.56E – 03	2.17E – 03	4.69E – 04	3.87E – 04
SMC	1.45E – 02	2.57E – 03	2.29E – 03	9.75E – 04	2.28E – 04	1.95E – 04
PER-SFC	**9.76**E-03	**1.19**E-03	**8.76**E-04	**4.16**E-04	**1.08**E-04	**9.72**E-05

Please cite this article in press as: Yang B, et al., Perturbation estimation based robust state feedback control for grid connected DFIG wind energy conversion system, International Journal of Hydrogen Energy (2017), http://dx.doi.org/10.1016/j.ijhydene.2017.06.222

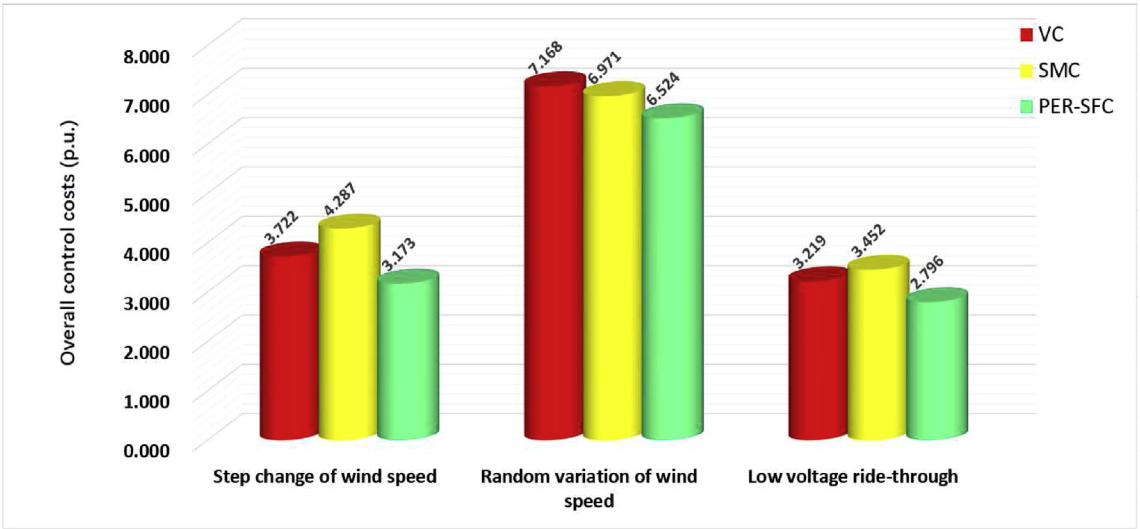

Fig. 9 – Comparison of overall control costs (in p.u.) of different controllers required in three scenarios.

to its merits of real-time perturbation compensation. In contrast, SMC has an inevitable over-conservative characteristics for the purpose of robust control. To summarize, PER-SFC outperforms other methods with satisfactory control performance and reasonable control costs.

Conclusions

This paper proposes a novel PER-SFC scheme to realize MPPT of DFIG, which has wisely incorporated the merits of conventional linear state feedback control, e.g., favourable implementation simplicity and high reliability, and nonlinear robust control, e.g., global control consistency and considerable robustness. Meanwhile, the inherent drawbacks of both control can be noticeably reduced. Due to the use of real-time perturbation estimation, only the measurement of rotor speed and reactive power is required thus PER-SFC can be easily implemented in practice. Case studies have been carried out which verify that the proposed approach is able to effectively achieve MPPT with the least power oscillations, rapidly restore the disturbed DFIG system during LVRT, provide similar robustness to SMC in the presence of parameter uncertainties, and require the lowest overall control costs. Future studies will focus on the hardware implementation of PER-SFC on an experimental DFIG system.

Acknowledgements

The authors gratefully acknowledge the support of National Basic Research Program of China (973 Program: 2013CB228205), National Natural Science Foundation of China (51477055,51667010), Yunnan Provincial Talents Training Program (KKSY201604044), and Scientific Research Foundation of Yunnan Provincial Department of Education (KKJB201704007).

REFERENCES

[1] Wang B, Mi ZF, Nistor I, Yuan XC. How does hydrogen-based renewable energy change with economic development? Empirical evidence from 32 countries. Int J Hydrogen Energy 2017. http://dx.doi.org/10.1016/j.ijhydene.2017.03.059.
[2] Kim M, Kim JY. An integrated decision support model for design and operation of a wind-based hydrogen supply system. Int J Hydrogen Energy 2017;42:3899–915.
[3] Hooper T, Beaumont N, Hattam C. The implications of energy systems for ecosystem services: a detailed case study of offshore wind. Renew Sustain Energy Rev 2017;70:230–41.
[4] Tamalouzt S, Benyahia N, Rekioua T, Rekioua D, Abdessemed R. Performances analysis of WT-DFIG with PV and fuel cell hybrid power sources system associated with hydrogen storage hybrid energy system. Int J Hydrogen Energy 2016;41:21006–21.
[5] Hamzaoui I, Bouchafaa F, Talha A. Advanced control for wind energy conversion systems with flywheel storage dedicated to improving the quality of energy. Int J Hydrogen Energy 2016;41:20832–46.
[6] Hachicha F, Krichen L. Rotor power control in doubly fed induction generator wind turbine under grid faults. Energy 2012;44:853–61.
[7] Li SH, Haskew TA, Williams KA, Swatloski RP. Control of DFIG wind turbine with direct-current vector control configuration. IEEE Trans Sustain Energy 2012;3(1):1–11.
[8] Yang B, Zhang XS, Yu T, Shu HC, Fang ZH. Grouped grey wolf optimizer for maximum power point tracking of doubly-fed induction generator based wind turbine. Energy Convers Manag 2017;133:427–43.
[9] Mehta B, Bhatt P, Pandya V. Small signal stability enhancement of DFIG based wind power system using optimized controllers parameters. Int J Electr Power Energy Syst 2015;70:70–82.
[10] Lawrence KL, Munda JL, Hamam Y. A fuzzy-PI controller for wind turbine driven DFIG optimized using genetic algorithms. In: Proceedings of 1st international conference on simulation and modeling methodologies, technologies and applications, Noordwijkerhout, The Netherlands; 2011. p. 29–31. July.

Please cite this article in press as: Yang B, et al., Perturbation estimation based robust state feedback control for grid connected DFIG wind energy conversion system, International Journal of Hydrogen Energy (2017), http://dx.doi.org/10.1016/j.ijhydene.2017.06.222

[11] Suryoatmojo H, Zakariya AMB, Anam S, Musthofa A, Robandi I. Optimal controller for doubly fed induction generator (DFIG) using differential evolutionary algorithm (DE). In: 2015 international seminar on intelligent technology and its applications (ISITIA), surabaya, Indonesia; 2015. p. 20–1. May 159-164.
[12] Chatterjee S, Naithani A, Mukherjee V. Small-signal stability analysis of DFIG based wind power system using teaching learning based optimization. Int J Electr Power Energy Syst 2016;78:672–89.
[13] Yang B, Jiang L, Wang L, Yao W, Wu QH. Nonlinear maximum power point tracking control and modal analysis of DFIG based wind turbine. Int J Electr Power Energy Syst 2016;74:429–36.
[14] Kahla S, Soufi Y, Sedraoui M, Bechouat M. On-Off control based particle swarm optimization for maximum power point tracking of wind turbine equipped by DFIG connected to the grid with energy storage. Int J Hydrogen Energy 2015;40:13749–58.
[15] Errouissi R, Al-Durra A, Muyeen SM, Leng S, Blaabjerg F. Offset-free direct power control of DFIG under continuous-time model predictive control. IEEE Trans Power Electron 2017;32(3):2265–77.
[16] Taveiros FEV, Barros LS, Costa FB. Back-to-back converter state-feedback control of DFIG (doubly-fed induction generator)-based wind turbines. Energy 2015;89:896–906.
[17] Evangelista CA, Valenciaga F, Puleston P. Multivariable 2-sliding mode control for a wind energy system based on a double fed induction generator. Int J Hydrogen Energy 2012;37:10070–5.
[18] Pena RR, Fernandez RD, Mantz RJ. Passivity control via power shaping of a wind turbine in a dispersed network. Int J Hydrogen Energy 2014;39:8846–51.
[19] Gao SH, Mao CX, Wang D, Lu JM. Dynamic performance improvement of DFIG-based WT using NADRC current regulators. Electr Power Energy Syst 2016;82:363–72.
[20] Guo WT, Liu F, Si J, He DW, Harley R, Mei SW. Approximate dynamic programming based supplementary reactive power control for DFIG wind farm to enhance power system stability. Neurocomputing 2015;170:417–27.
[21] Yang B, Jiang L, Yao W, Wu QH. Perturbation estimation based coordinated adaptive passive control for multimachine power systems. Control Eng Pract 2015;44:172–92.
[24] Qiao W. Dynamic modeling and control of doubly fed induction generators driven by wind turbines. In: 2009 IEEE/PES power systems conference and exposition, seattle, WA, mar. 15-18; 2009. p. 1–8.
[25] Fei M, Pai B. Modal analysis of grid-connected doubly fed induction generators. IEEE Trans Energy Convers 2007;22:728–36.
[26] Juan R, Edgar L, Vicente V, David C, Ramon A, Luis E. Current-sensorless control of an SPWM H-Bridge-based PFC rectifier designed considering voltage sag condition. Electr Power Syst Res 2016;130:181–91.
[27] Beltran B, Benbouzid MEH, Ahmed-Ali T. Second-order sliding mode control of a doubly fed induction generator driven wind turbine. IEEE Trans Energy Convers 2012;27(2):261–9.
[28] Rashid G, Ali MH. Nonlinear control-based modified BFCL for LVRT capacity enhancement of DFIG-based wind farm. IEEE Trans Energy Convers 2017;32(1):284–95.
[29] Yang B, Sang YY, Shi K, Yao W, Jiang L, Yu T. Design and real-time implementation of perturbation observer based sliding-mode control for VSC-HVDC systems. Control Eng Pract 2016;56:13–26.

Please cite this article in press as: Yang B, et al., Perturbation estimation based robust state feedback control for grid connected DFIG wind energy conversion system, International Journal of Hydrogen Energy (2017), http://dx.doi.org/10.1016/j.ijhydene.2017.06.222